Sheffield Hallam University

Local membrane length conservation in two-dimensional vesicle simulation using multi-component lattice Boltzmann Equation Method.

HALLIDAY, Ian, LISHCHUK, Sergey, PONTRELLI, G. and EVANS, P. C

Available from Sheffield Hallam University Research Archive (SHURA) at:

http://shura.shu.ac.uk/13050/

This document is the author deposited version. You are advised to consult the publisher's version if you wish to cite from it.

Published version

Repository use policy

Sheffield Hallam University Research Archive
http://shura.shu.ac.uk

Local Membrane Length Conservation in Two-Dimensional Vesicle Simulation using Multi-Component Lattice Boltzmann Equation Method.

I. Halliday, S. V. Lishchuk, T. J. Spencer, G. Pontrelli* and P. C. Evans**,

Materials & Engineering Research Institute, Sheffield Hallam University, Howard Street, S1 1WB (UK)

* Istituto per le Applicazioni del Calcolo - CNR, Via dei Taurini 19 - 00185 Roma (Italy)

** Department of Cardiovascular Science, and Insigneo Institute of In Silico Medicine, University of Sheffield Medical School, Beech Hill Road, Sheffield, S10 2RX

Corresponding Author: I. Halliday
Email address: i.halliday@shu.ac.uk
Telephone: (+44) 114 225 3045
Fax: (+44)114 225 3501

Abstract

We present a method for applying a class of velocity-dependant forces within a multi-component lattice Boltzmann equation simulation which is designed to recover continuum regime incompressible hydrodynamics. This method is applied to the problem, in two dimensions, of constraining to uniformity the tangential velocity of a vesicle membrane implemented within a recent multi-component lattice Boltzmann simulation method, which avoids the use of Lagrangian boundary tracers. The constraint of uniform tangential velocity is carried by an additional contribution to an immersed boundary force, which we derive here from physical arguments. The result of this enhanced immersed boundary force is to apply a physically appropriate boundary condition at the interface between separated lattice fluids, defined as that region over which the phase-field varies most rapidly. Data from this enhanced vesicle boundary method are in agreement with other data obtained using related methods (e.g. T. Krüger, S, Frijters, F. Günther, B. Kaoui and J. Harting, Eur. Phys. J. 222, 177 (2013))) and underscore the importance of a correct vesicle membrane condition.

1 Introduction

The non-Newtonian flow properties of blood emerge from the behaviour of its cellular constituents and the appropriately aggregated physics of cell deformation and lubrication flow must ultimately explain its description using power-law approximations [1] etc. The principal cellular component of blood comprises approximately 40% of its volume and is made-up of red blood cells, or erythrocytes, of 7μ diameter, which are, therefore, continuum-scale objects. Incorporating the fundamental physics and dynamics of this cellular length-scale into our understanding of the flow properties of blood is clearly an essential precursor to a correct description of continuum-scale haemodynamics. Indeed, the physically discrete micro-structure of blood necessarily implies that important modalites are coarse-grained out of any continuum description e.g. the fluctuating nature of wall shear stress (WSS) and its temporal and micro-spatial distribution at the arterial lumen, which is believed to condition endothelial cell shape and behaviour. In this article we will show that the micro-distribution of WSS may be affected by the effective boundary condition governing the embedded motion of the principal cellular component of blood i.e. erythrocytes.

Physically, erythrocytes are deflated vesicles, filled with incompressible liquid and bounded by lipid bi-layers, or membranes. Like fluid viscosity and interfacial tension, the physical properties of a vesicle membrane (surface tension, bending ratio and interfacial compressibility etc.) all originate at the molecular micro-scale but they may be incorporated into a continuum-scale description by an effective hydrodynamic boundary condition based upon an immersed boundary force distribution [2]. In this and other work located at the continuum scale e.g. [3, 9] the vesicle membrane is regarded as a deformable, impermeable boundary separating two immiscible Newtonian fluids with conserved cross-sectional area, an unsteady conformation responsive to flow stresses, which mediates stress boundary conditions between the segregated fluids.

Our previous membrane model [10] was based upon immiscible, multi-component lattice Boltzmann equation (MCLB) hydrokinetics. That model is capable of producing correct vesicle conformations and hydrodynamic boundary conditions over a wide range of parameter, but since it employs a force distribution which is constrained by global membrane length conservation, the physical effect of uniform tangential motion in the vesicle membrane is not recovered. An important consequence of this lost interfacial modal-

ity is the phenomenon of vesicle tank-treading. We note that tank treading motion is also observed in 2D droplets and capsules. In the case of vesicles however it results in a constant value of the tangential velocity over the length of the membrane which it is particularly important to recover. In the rest of this article, the term tank-treading refers to a vesicle motion in which all points on the boundary move with the same tangential velocity. The limited aim here is to close the physical content of our previous model and, as indicated above, provide an illustration of the physiological importance of an advance which brings the present model into line with others [5,7], [9]. The additional physical content will arise as a result of vesicle membrane *element* length conservation which, in turn, arises from a newly postulated, physical force distribution which is velocity-dependant- a fact which introduces certain complications.

The extended method we report inherits the ability efficiently to deal with large numbers of intimately-interacting but separate vesicles from its pre-cursor [10] and earlier memory-efficient, coalescence-controlling MCLB methods for multiple liquid drops [11], [12]. Moreover, it requires no computational re-meshing and it is founded solely on a distribution function-based technique, requiring no embedded system of connected Lagrangian points. However MCLB is effectively an unsteady Navier-Stokes solver and as such it requires the definition of explicit boundary conditions, so our methods are unable exactly to recover the $Re = 0$ Stokes regime, the effects of vesicle confinement cannot be removed and it cannot be efficiently applied to the problem of interrogating vesicle phase spaces [7]. Indeed, it can be advantageously distinguished from the very accurate boundary integral formulations of fluid dynamics used by other workers only by its ability conveniently to treat large numbers of interacting vesicles flowing in complex geometry [12].

For flow containing a membrane constrained to have uniform tangential velocity the hydrodynamic boundary condition may not appear to change significantly relative to that implicit in our previous MCLB model, which relied on global membrane length conservation, recall. Certainly, for steady flow in 2D the vesicle boundary is a streamline in both models. The extent to which a constraint of uniform membrane tangential velocity affects vesicle dynamics is therefore unclear and a question arises as to the physical and physiological impact of an enhanced effective boundary motion. We will present limited evidence which suggests that the increased model complexity and computational load is justified. It is appropriate however to remember from the outset, a constraint of local membrane length element conservation,

2

when extended to three dimensions, becomes one of constant local membrane area. In the latter case, incompressible surface flows are possible which are ruled-out in two-dimensional models. We also neglect the local cytoskeleton present in e.g. erythrocytes [13] which imparts a local viscoelasticity (though account could possibly be taken of this effect [14]) and a global effect of shape memory, due to the presence of a spectrin network [15].

This article is set-out as follows. Section 2 reviews relevant features of our previous method, in section 3 we consider examples of velocity-dependant forces in hydrokinetic simulation, in section 4 we derive an appropriate physical force to carry local membrane length element conservation and in section 5 we consider how this force might be impressed on lattice fluid, within MCLB, in section 6 we present and discuss results and in section 7 our conclusions. For simplicity we consider throughout a single vesicle. However, we emphasise that the methods we report apply directly to multiple vesicle simulations, without modification.

2   Background

Previously we generalised an established MCLB method designed to recover Laplace law behaviour, based upon Lishchuk's method [16], so that the physical properties of the interface between two completely immiscible flowing fluids are consistent with a membrane of globally conserved length, preferred curvature, specified interfacial tension and bending rigidity. [10]. In this method, membrane physics and associated fluid kinematic effects arise from a curvature and length dependent force density, impressed in regions where the fluid components' phase-field, ρ^N, varies most rapidly. In this method, only distribution functions are required to carry the membrane information and no other computational elements such as a Lagrangian mesh are required. In this section we outline those elements of this model central to the task of extending it to contain local membrane element length conservation.

Let two fluid distributions occupying lattice link i, at position $\underline{r}$ to be described by distribution functions, $R_i(\underline{r})$ and $B_i(\underline{r})$ (of course with $f_i(\underline{r}) = R_i(\underline{r}) + B_i(\underline{r})$). The nodal density of the red and blue fluids:

$$\rho_R(\underline{r}) = \sum_i R_i(\underline{r}), \quad \rho_B(\underline{r}) = \sum_i B_i(\underline{r}), \tag{1}$$

3

is used to define a local phase field [17]:

$$\rho^N(\underline{r}) = \frac{\rho_R(\underline{r}) - \rho_B(\underline{r})}{\rho_R(\underline{r}) + \rho_B(\underline{r})}. \tag{2}$$

Surfaces $\rho^N = constant$ define the interface with $\rho^N = 0$ its centre. Throughout the narrow but distributed interfacial region, the local interface normal is obtained from numerical approximations for the following:

$$\hat{\underline{n}} = -\frac{\nabla \rho^N}{|\nabla \rho^N|}. \tag{3}$$

With the above definition, for a red drop in a blue fluid, the interface normal unit vector, $\hat{\underline{n}}$ points away from the enclosed red fluid. Local interfacial curvature is obtained from the surface gradient of $\hat{\underline{n}} = (\hat{n}_x, \hat{n}_y)$, which, in two-dimensions, is [16] given by:

$$\kappa \equiv \hat{n}_x \hat{n}_y \left(\frac{\partial \hat{n}_y}{\partial x} + \frac{\partial \hat{n}_x}{\partial y} \right) - \hat{n}_y^2 \frac{\partial \hat{n}_x}{\partial x} - \hat{n}_x^2 \frac{\partial \hat{n}_y}{\partial y}. \tag{4}$$

All the derivatives in equations 3 and 4 are usually computed to $o(\underline{c}_i^4)$ accuracy with a simple, local, compact stencil:

$$\frac{\partial \phi}{\partial x_\alpha} = \frac{1}{k_2} \sum_{i \neq 0} t_i \phi(\underline{r} + \underline{c}_i) c_{i\alpha} + O(\underline{c}_i^4), \quad \alpha \in [x, y], \tag{5}$$

where the lattice isotropy constant $k_2 = c_s^2 = 1/3$ for the $D2Q9$ lattice used here, ϕ denotes any field variable and t_i is the lattice link weight with $t_i = 4/9$ for $|\underline{c}_i| = 0$, $t_i = 1/9$ for $|\underline{c}_i| = 1$ and $t_i = 1/36$ for $|\underline{c}_i| = \sqrt{2}$. Clearly, the number of grid-points required to calculate a gradient depends upon the cardinality of the LBE lattice unit cell's basis set, Q, as well as other considerations, to be discussed.

The effects of the a membrane emerge in simulations from the application of the following normally-directed, weighted body force density at the boundary between the two fluids:

$$\underline{F}^{(0)} = \frac{1}{2}\nabla \rho^N \left(\kappa \left(\sigma - \alpha_0 \left(1 - \frac{l}{l_0} \right) \right) - \frac{b}{2}\kappa \left(\kappa^2 - \kappa_0^2 \right) - b\frac{\partial^2 \kappa}{\partial s^2} \right). \tag{6}$$

Here $\frac{1}{2}\nabla \rho^N$ is the weight [16], κ (κ_0) is the (preferred) interfacial curvature, α_0 the interfacial compressibility, σ an interfacial tension further discussed

4

below, l (l_0) the (reference) length of the interface and b its bending rigidity. In the above, s denotes distance measured along the direction of the membrane. This purely normal force is derived from a free energy density [10].

The already complex MCLB immersed boundary force density in equation 6 does not produce a membrane tank-treading motion. However, it has been shown to recover appropriate vesicle shapes and dynamics, for the continuum regime [10] i.e using that force density in equation 6, there results an equilibrium shape which is consistent with a constant enclosed volume, membrane cross-sectional area (length in 2D), membrane preferred curvature and interfacial tension, which may nevertheless be deformed when external traction is applied, as the embedding fluid flows. Note that the constraint of constant vesicle volume is automatic as long as the enclosed fluid is incompressible. Note also that immersed boundary forces are known to be responsible for inducing unphysical, spurious flow in MCLB models and that correct interfacial kinematics arise from an appropriate segregation step [18]. So, for example, the kinematic property of mutual impenetrability emerges from correctly-chosen, post-collision colour segregation rules, [10], developed from the work of d'Ortona et.al. [18]. We shall return to the segregation scheme in section 4, below.

Figure 1 illustrates the essential problem with the MCLB identified by that force density in equation 6. This data was obtained for an unsteady flow containing a deflated, sheared vesicle. It shows the velocity of the vesicle membrane (top panel) resolved onto the local tangent with the effective solid-body rotation removed, note. Clearly visible in the lower panel is a significant variation of the membrane tangential velocity. Physically correct motion requires all points on the membrane to move with the same instantaneous speed in the direction of the local membrane tangent, viewed from the rest-frame of the vesicle.

Before proceeding, we compare the body force density in equation 6 with others in the literature. Equation 6 corresponds to one possible separation of interfacial effects: our constant interfacial tension σ is a curvature independent contribution to a membrane free energy density per unit area of surface [19], which may be small for physical membranes. Salac uses an interfacial tension γ in a similar way [20], also within an Eulerian method using level-set tracking. Parameter σ does not appear as a Lagrange multiplier, introducing the constraint of local length element conservation, as in the work of Kaoui et. al. [5, 7] (which is now widely implemented, including within lattice Boltzmann [21], [22]). Rather, global length conservation

5

(only) here arises as a consequence of continually adjusting a uniform interfacial tension $(\sigma - \alpha_0(1 - \frac{l}{l_0}))$ and the surface tension is constant over the membrane. In the last expression, α_0 may be considered as a physical interface compressibility [10], which unfortunately does not achieve zero change in a local membrane length element. We will use physical arguments to devise a remedial force distribution which has a tangential component and which may be argued to function practically in a manner similar to Salac's tangential gradient in interfacial tension, $\nabla_s \gamma$, [20] and to Kaoui's Lagrange multiplier [5, 7].

Now, the membrane force in equation 6 is applied as an external force density to what is effectively a single lattice fluid described by distribution function $f_i = R_i + B_i$. He et al. [23] and Guo et al. [24] generalized the LBGK model, originally devised by Qian et. al. [25], to describe lattice fluid subject to a known, spatially variable external force density, $\underline{F}$. Collision and forcing of the distribution function when the system is close to equilibrium, note, is:

$$f_i^\dagger = f_i^{(0)}(\rho, \rho\underline{v}) + \left(1 - \frac{1}{\tau}\right) f_i^{(1)}(\nabla\rho, ..\partial_x v_y.., \underline{F}) + F_i(\tau, \underline{F}, \underline{v}), \qquad (7)$$

where the dagger superscript indicates a post-collision, pre-propagate quantity, $f_i^{(0)}(\rho, \underline{v})$ denotes the equilibrium distribution function [29] and the source term, F_i is [23], [24] :

$$F_i = t_i \left(1 - \frac{1}{2\tau}\right) \left(\frac{(\underline{c}_i - \underline{v})}{c_s^2} + \frac{(\underline{c}_i \cdot \underline{v})(\underline{c}_i)}{c_s^4}\right) \cdot \underline{F}, \qquad (8)$$

where all symbols have their usual meaning. In the presence of any external force $\underline{F}$, the value of the fluid velocity depends upon that external force [23], [24] :

$$\underline{v} = \frac{1}{\rho} \sum_i f_i \underline{c}_i + \frac{1}{2\rho} \underline{F}. \qquad (9)$$

In summary, in the above method all the dynamics and kinematics is embedded within a force distribution and the fluids' phase field: it requires no set of constrained Lagrangian points to indicate the location of its interface. The extensions developed here preserve this property. It is clear from equation 9 however that a question arises when the external force depends upon the fluid velocity, as is the case in e.g. magnetohydrodynamics, geophysical flows as well as in vesicle hydrodynamics. We consider this matter in more detail now.

3 Velocity-Dependant Forces in Lattice Boltzmann Simulation

The problem of encapsulating velocity-dependant forces in the LB method i.e. solving equation 9 for $\underline{v}$ may be achieved in different ways, depending upon the complexity of the force and its physical origin.

Within the two-dimensional f-approximation of geophysical flow, with the z-axis taken as locally parallel to $\underline{g}$, the effective Coriolis acceleration acing upon a two-dimensional fluid (i.e a shallow layer) is given by:

$$\underline{F}(\underline{v}) = \underline{\Omega} \times \underline{v} = (-\Omega_z v_y, \Omega_z v_x, 0),\tag{10}$$

where all symbols have their usual meaning. Using equation 9, the velocity field of a lattice fluid subject to a Coriolis force may be obtained explicitly, by inverting the following system of equations using straightforward linear algebra:

$$\left[\begin{array}{cc} \rho & \frac{\Omega_z}{2} \\ -\frac{\Omega_z}{2} & \rho \end{array}\right] \times \left[\begin{array}{c} v_x \\ v_y \end{array}\right] = \sum_i f_i \left[\begin{array}{c} c_{xi} \\ c_{yi} \end{array}\right].\tag{11}$$

In other cases, it is not so straightforward to introduce a velocity-dependant force. Guo and Zhao who were first to recognise and address the problem of finding explicit solutions to equation 9 [26] considered LB models of porous flow using a velocity-dependant force due to Nithiarasu [28], $\underline{F}(\underline{v}) = \frac{\epsilon\nu}{K}\underline{v} - \frac{\epsilon F_\epsilon}{\sqrt{K}}|\underline{v}|\underline{v} + \epsilon\underline{G}$, which, when substituted into equation 9, gives the following quadratic for $|\underline{v}|$: $c_1|\underline{v}|^2 + 2c_0|\underline{v}| - \underline{V} = 0$, where $\underline{V} \equiv \sum_i f_i\underline{c}_i + \frac{\rho\epsilon}{2}\underline{G}$, $c_1 = \frac{\epsilon F_\epsilon}{2\sqrt{K}}$, $c_0 = \frac{1}{2}\left(1 + \frac{\epsilon\nu}{2K}\right)$. Taking the positive root of the above, Guo and Zhao find an explicit expression for $\underline{v}$ in this model of porous flow:

$$\underline{v} = \frac{\underline{V}}{c_0 + \sqrt{c_0^2 + c_1|\underline{V}|}}.\tag{12}$$

Clearly therefore, some cases of velocity-dependant forces in fluid dynamics could be approached using forced LB simulation directly

Next consider the case of $\underline{F} = \underline{F}(\underline{v}, \underline{\nabla}.\underline{v}..)$. If it is possible to write $\underline{F}(\underline{v})$ in finite differences with constant coefficients, then equation 9 might generate a system of linear equations, the numerical or analytical solution of which might be possible, though costly.

The more complex and inter-dependant force distribution required to eliminate tangential gradients of membrane velocity is not so amenable to

analysis as the examples above. A more elaborate, iterative procedure is necessary. We continue by considering an additional, velocity-dependant force contribution $\underline{F}'(\underline{v})$ which is (i) effectively linear (ii) small relative to the principal forces, $\underline{F}^{(0)}$, acting and (iii) small relative to its argument in the following sense:

$$
\begin{aligned}
\underline{F}'(\underline{v} + \underline{w}) &= \underline{F}'(\underline{v}) + \underline{F}'(\underline{w}), &(13) \\
\frac{|\underline{F}'(\underline{v})|}{|\underline{F}^{(0)}|} &= O(\delta), \\
\frac{|\underline{F}'(\delta\underline{v})|}{|\underline{F}^{(0)}|} &= O(\delta^2), \\
&etc.
\end{aligned}
$$

Here label δ is used as a measure of magnitude with $\delta < 1$ assumed. Write $\underline{v} = \underline{v}^{(0)} + \delta\underline{v}^{(1)} + \delta^2\underline{v}^{(2)} + ...$ The total force acting at time t is given by the sum expression $\left(\underline{F}^{(0)} + \underline{F}(\underline{v}(t))\right)$. From equation 8 therefore:

$$
\underline{v}^{(0)} + \sum_j \delta^j \underline{v}^{(j)} = \frac{1}{\rho} \sum_i f_i \underline{c}_i + \frac{1}{2\rho}\underline{F}^{(0)} + \frac{1}{2\rho}\underline{F}'\left(\underline{v}^{(0)} + \sum_j \delta^j \underline{v}^{(j)}\right), \quad (14)
$$

and using the assumed properties in equations 13 we equate powers of parameter δ to obtain, at lowest order:

$$
\underline{v}^{(0)} = \frac{1}{\rho} \sum_i f_i \underline{c}_i + \frac{1}{2\rho}\underline{F}^{(0)}. \quad (15)
$$

In our case $\underline{F}^{(0)}$ is the principal membrane force given in equation 6. At higher order in δ:

$$
\delta^j \underline{v}^{(j)} = \frac{1}{2\rho}\underline{F}'(\underline{v}^{(j-1)}), \quad j > 0. \quad (16)
$$

Once a membrane velocity gradient constraining force has been defined, in the next section, we shall use equations 15 self-consistently to incorporate its effects.

4 Force Distribution for Local Membrane Length Conservation

In previous work we presented an algorithm which conserved the global length of membrane [10]. Here we use physical arguments and assumptions about

the properties of a membrane to derive an additional force distribution which tends to conserve length in any one element of a two dimensional boundary. This extra contribution is obtained by determining the physical force associated with extension or compression of an element of the bounding membrane about its unstrained equilibrium length. Application of this additional force contribution to the interfacial fluid will then introduce the constraint of uniform tangential boundary motion. Put another way, a physical force will now enforce local length element conservation, embedding tank-treading, in the emergent dynamics of the system of internal, external and interfacial fluid.

Consider the material derivative of an elongated boundary length element of unstrained length δl_0, stretched between $\underline{r}_1 = (x_1, y_1)$, $\underline{r}_2 = (x_2, y_2)$ where the fluid velocity is $\underline{v}_1$, $\underline{v}_2$, respectively. After some algebra we find:

$$\frac{D}{Dt}\delta l = \hat{t} \cdot (\underline{v}_2 - \underline{v}_1) = v_{t2} - v_{t1}. \tag{17}$$

Here $\underline{\delta l} = \underline{r}_2 - \underline{r}_1$ and $\underline{\delta l}/\delta l = \hat{t}$. Let us now assume Hookean behaviour of the membrane material and write $\delta l = (1 + \epsilon)\delta l_0$ hence:

$$\frac{D\epsilon}{Dt} = \frac{(v_{t2} - v_{t1})}{\delta l_0} = \frac{\partial v_t}{\partial s}, \tag{18}$$

where s denotes distance measured along the membrane. Using the definition of the material derivative following the motion, we arrive at a partial differential equation governing the evolution of strain in a Hookean membrane:

$$\frac{\partial \epsilon}{\partial t} = \frac{\partial v_t}{\partial s} - v_x \frac{\partial \epsilon}{\partial x} - v_y \frac{\partial \epsilon}{\partial y}, \tag{19}$$

Let us now consider the corresponding force distribution. The unbalanced force acting within the length element under consideration is:

$$\underline{\delta F} = \left[k\epsilon\delta l\hat{t}\right]_{\underline{r}_2} - \left[k\epsilon\delta l\hat{t}\right]_{\underline{r}_1} = k\delta l\underline{dr} \cdot \underline{\nabla}\left(\epsilon\hat{t}\right), \tag{20}$$

where $\underline{dr} = \underline{r}_2 - \underline{r}_1$, k is the membrane spring constant and $\hat{t}$ is the unit vector tangent to the membrane, whence:

$$\underline{\delta F} = k\delta l\frac{\partial}{\partial s}\left(\epsilon\hat{t}\right) = k\delta l\epsilon\frac{\partial \hat{t}}{\partial s} + k\delta l\hat{t}\frac{\partial \epsilon}{\partial s}, \tag{21}$$

which, on using the Frenet-Seret formulae gives the following velocity-dependant force per unit length of membrane for ensuring a uniform tangential motion

9

of the membrane: $\frac{\delta F}{\delta l} = \left(k\epsilon\kappa\hat{n} + k\frac{\partial\epsilon}{\partial s}\hat{t}\right)$. This force, which has a tangential component, note, must be applied as a body force to the lattice fluid which occupies the interfacial region, with exactly the same weight as that used in equation 6:

$$\underline{F}'(\underline{v}) = \frac{1}{2}\left|\nabla\rho^N\right|\left(k\epsilon\kappa\hat{n} + k\frac{\partial\epsilon}{\partial s}\hat{t}\right). \tag{22}$$

In the body force above, strain ϵ must be obtained by solving equation 22. This force density is velocity-dependant through $\epsilon = \epsilon(\underline{v})$. We assume that k is large i.e. the membrane strongly resists compression and may be expected to relax any strains very rapidly, compared with the timescales characteristic of the flow, to a state of uniform strain. We note that the interface compressibility term in equation 6 is *not* now omitted $\alpha_0 \neq 0$. The physical effect of $\underline{F}'$ is to homogenise the strain distribution within a membrane of given length but that length is regulated in part by the term in α_0 in equation 6.

Before proceeding, we suppose equation 18 may be accurately integrated for a finite time along a characteristic line to give $\Delta(\delta l) = \frac{\partial v_t}{\partial s}\Delta t$. From this expression we can approximate the force generated by this strain as $\Delta F' = k\frac{\partial v_t}{\partial s}\Delta t$. This crude argument supports the underlying linearity property of $\underline{F}'$ assumed in section 3

5   Multi-Component Lattice Boltzmann Scheme

Care must be taken in the integration of equation 19. Using the trapezium rule, an implicit scheme with up-winding for those terms corresponding to the spatial derivatives of velocity is:

$$
\epsilon_{ij}^{(n+1)} = \epsilon_{ij}^{(n)} \quad - \quad D_x\left(\frac{v_{xij}^{(n)} + v_{xij}^{(n+1)}}{2}\right) D_x\left(\frac{\epsilon_{xij}^{(n)} + \epsilon_{xij}^{(n+1)}}{2}\right)\delt \tag{23}
$$

$$
- \quad D_y\left(\frac{v_{yij}^{(n)} + v_{yij}^{(n+1)}}{2}\right) D_y\left(\frac{\epsilon_{yij}^{(n)} + \epsilon_{yij}^{(n+1)}}{2}\right)\delt
$$

$$
+ \quad D_s\left(\frac{v_{ts}^{(n)} + v_{ts}^{(n+1)}}{2}\right)\delt.
$$

Here $D_\alpha(f)$ denotes an upwind numerical derivative of the quantity f. No confusion should arise between the introduction of spatial position subscript

j and the velocity correction index (j), which is used as a superscript. Together, equations 19, 23 (expressed in finite differences) and 8 form a complicated system of equations from which, in principle, the $\epsilon_{ij}^{(n+1)}$ may be eliminated and $v_{ij}^{(n+1)}$ determined. Bearing in mind the discussion of section 3 however, we must take a different approach evolving self-consistent instantaneous strain, $\epsilon_{ij}^{(n+1)}$, and lattice velocity $\underline{v}$.

The following (annotated) steps were used to compute the velocity-dependant component of membrane force, $\underline{F}'(\underline{v})$ in each MCLB time step. Beginning from the post-collision state at time n, for the whole lattice:

1. propagate,

2. compute the principal force contribution, $\underline{F}_{ij}^{(0)}$, using equation 6,

3. estimate $\underline{v}_{ij}^{(n+1)}$ using equation 15,

4. estimate $\epsilon_{ij}^{(n+1)}$ from the last estimate of $\underline{v}_{ij}^{(n+1)}$ using equation 16 (**Remark** initially, use the $\underline{v}_{ij}^{(n+1)}$ from step (3) above.),

5. compute velocity-dependant force contribution $\underline{F}'$, using equations 5 and 19,

6. correct $\underline{v}_{ij}^{(n+1)}$ (**Remark** equation 16 now implies that change to the velocity used in steps (3)..(5) which we have denoted $\delta^j \underline{v}^{(j)}$.),

7. if $\max |\delta^j \underline{v}^{(j)}|$ is larger that 1% return to (4),

8. collide the lattice.

The data presented in the next section become insensible to further iteration, once steps (4)..(7) have been repeated 5 times, with an average of about three iterations necessary to satisfy the criterion in (6). The algorithm above is essential to the stability of our MCLB method with a velocity-dependant membrane force contribution: with those parameters considered in the next section, stable simulations are impossible without their use, probably because the relative magnitude of an effective force correction is large.

Let us consider dimensionless ratio:

$$R(j) = \lim_{t \to \infty} \left(\left\langle \frac{|\delta^j \underline{v}^{(j)}|}{|\delta^0 \underline{v}^{(0)}|} \right\rangle_{ij} \right), \quad j \in [1, 5] \tag{24}$$

11

where angle brackets indicate an average taken over that part of space occupied by the membrane i.e. on a range of the subscripts i, j. Table 1 below illustrates the convergence of the overall membrane force, measured by $R(n)$ as defined in equation 24. Note that it follows from the data in table 1 that the first estimate of correction $|\underline{F}'|$ is large, (being approximately $|\underline{F}_0|/2$, with $\underline{F}_0$ defined in equation 6).

The scheme defined in this section constrains the tangential motion of the interface only in a statistical sense, as we now discuss. We have indicated that, in most MCLB, the interface between fluids is smoothly distributed with interface-normal distance, n. Viewed as a function of n, ρ^N has a variation:

$$
\rho^N(n) \sim \tanh(\beta n) \iff n \sim \frac{1}{\beta} \tanh^{-1}\left(\rho^N\right).
\tag{25}
$$

Here β an adjustable segregation parameter ($\beta = 0.67$ in the present work) and the interface is assumed to be stationary. (The variation in equation 25 above was shown in [10] to arise as a consequence of using the segregation scheme of d'Ortona et.al. [18]). Hence the weight in equations 6 and 22 has a normal variation which may be expressed as follows:

$$
\frac{1}{2}|\underline{\nabla}\rho^N| = \frac{\beta}{2}\left(1 - \rho^{N2}\right),
\tag{26}
$$

our constraint force in equation 22 will be distributed (with a peak intensity at the centre of the interface, $\rho^N = 0$) and we expect v_t will vary in the normal direction. To illustrate this consider how v_t varies with the curvilinear coordinate tangential to the membrane, at chosen values of n. In figure 2, we present data for a sheared vesicle of approximate deflation 0.83, filled with fluid of the same viscosity as that of the exterior fluid. The value of the tangential velocity in the interfacial region was interpolated onto sub-lattice contours $\rho^N = 0, \pm 0.585, \pm 0.872, \pm 0.965$ (which correspond to distance $n = 0, \pm 1, pm2, \pm 3, \pm 4$ respectively) to form data sets characterised by a value of ρ^N as effective normal coordinate. The mean, μ, and standard deviation, σ, of these data sets is plotted against ρ^N in figure 2. This data supports the conclusion that membrane's tangential velocity is well-defined and constant along contour $\rho^N = 0$, at its centre. However, along parallel contours there is more variation.

6   Results and Discussion

A tank-treading of a vesicle membrane is clearly inconsistent with motion in certain geometries. For instance, the membrane of a two-dimensional vesicle which is propelled along the centre of a duct, by a pressure gradient or body force, must move with the same velocity at all points- that of the centre of mass of the vesicle. In this section we study motions which allow for tangential motion of the membrane, the simplest being a shear flow. All the data presented corresponds to $k = 1$, large: a value was determined by progressively increasing k, until our results were insensible to further change.

Results from the present model compare favourably with others, once the force distribution $\underline{F}'$ is installed. We consider the change from tank-treading to tumbling motion, which has been carefully studied for bounded flow by Kaoui et. al. who studied confinement effects [21] and the effect of a viscosity contrast [22]. In 2013, Krüger et. al. reported the result of a simulations performed with LBM-FEM [30], performed on a moderately deflated 2D vesicle with confinement, at two values of viscosity contrast parameter:

$$\Lambda \equiv \frac{\eta_2}{\eta_1}, \tag{27}$$

where η_2 (η_1) denotes the vesicle interior (exterior) fluid viscosity. In Fig. 3 of reference [30] , Krüger et. al. summarise, for a vesicle in the $x - y$ plane, subjected to a shear in the x direction (i) a tank-treading behaviour for $\Lambda = 1$ and (ii) a tumbling motion for $\Lambda = 12$. To validate, we match the deflation parameter and system size to the data of this figure and non-dimensionalizing time in the same way (using the unperturbed shear rate, $\dot{\gamma}$), we obtain the responses shown in figure 3 below, which agree well. Inclination angle θ, is the angle subtended at the horizontal (i.e. unperturbed flow direction), of the long-axis of the vesicle. As shown by Krüger et. al., the vesicle orientates at positive θ in tank-treading but it rotates unsteadily with $\frac{d\theta}{dt} < 0$ when tumbling. Physically, these two motions accord, respectively, with the behaviour of an immiscible drop and an almost-rigid particle which acquires angular momentum (due here to the persistent uniform motion of its boundary) and so is induced to rotate in a direction consistent with the applied shear. We note that intermediate values of $\Lambda \in [1, 12]$ may also show tumbling, depending upon the values of deflation. While a full investigation of these effects is beyond present scope, it is appropriate briefly to consider membrane velocity, v_t, as function of Λ and θ in our model next.

13

Beaucourt et. al., [27] studied steady and unsteady dynamics in a vesicle. Here, we only consider v_t as a function of angle θ for particular cases of sheared systems with finite lattice Reynolds number, based upon exterior fluid's kinematic viscosity (or LB collision parameter, τ_1):

$$Re \equiv \frac{(\dot{\gamma}^* a^*) a^*}{\nu^*} = 1.8, \quad \nu^*(\tau_1) = \frac{1}{6} \left(2\tau_1 - 1\right), \quad (28)$$

where asterisks denote dimensionless lattice quantities and a^* is the largest vesicle dimension. First we consider deflated, tumbling vesicles with $\Lambda = 1$, second more circular, tank-treading vesicles at a range of $\Lambda \in [1, 2.5]$. Specifically, in figure 4 we plot v_t with θ for two collapsed vesicles, with deflations of $\alpha = 0.7, 0.8$, $\Lambda = 1$. The two sets of data in this figure show qualitatively similar variation, note. In figure 5 we consider more circular vesicles with $\alpha = 0.93$ at a range of $\Lambda \in [1, 2.5]$, which reach a steady inclination (computations were suspended when $\frac{d\theta}{dt} = 0$).

The remainder of our results all relate to a deflated vesicle i.e. one at a smaller value of α, and emphasise the importance of a membrane boundary condition $v_t = constant$. Recall, figure 1 shows the variation over the membrane, or interface, of v_t for a particular orientation of the long axis of the vesicle. v_t is calculated in the vesicle rest frame, viewed from which its membrane should, even in unsteady flow, now move with a tangential velocity component which is constant along its length. We further compare the vesicle dynamics with and without the effects of body force density $\underline{F}'$, focusing upon the fluid dynamics of the interaction of the vesicle with a solid boundary, at short length and time-scales.

A physiological parameter affected by the modifications developed here is the wall shear stress (WSS), which is important in e.g. the study of atherosclerosis. We consider a proxy WSS signal at the surface of the lumen or $y = 0$ boundary, for a single vesicle transit, with and without local length conservation i.e. for a vesicle membrane which can move like the interface between immiscible liquids and one subject to constraining force $\underline{F}'$. In figures 6 and 7 we show data for 2D vesicles with approximate deflation 0.65, bending rigidity $b = 1.4$ and interfacial tension $\sigma = 0.004$ (all expressed in lattice units) as they pass close to a flat, no–slip boundary, occupying $x = 0$. The figures compare WSS signals i.e. stress component $\eta \frac{\partial v_x}{\partial y}$ for equivalent angular orientations with and without global membrane length conservation. For this data, the simulation box size measured in lattice units is 130×130, the viscosity contrast between interior and exterior fluids is

14

$\Lambda = 12$ and the local lattice Reynolds number $Re = 0.98$. This value of Re ensures that micro-currents generated by the complex immersed boundary forces are small compared with flow velocity. Of course, other values of Re small or large may be addressed with this method, subject to the following consideration. It is necessary to ensure that the interfacial micro-current for the chosen parameterisation is insignificant compared with the flow velocities over the majority of the domain. In figure 6 we show a WSS signal for an orientation of a translating and rotating vesicle for which the deflated vesicle's long axis is approximately parallel to the streamlines of undisturbed flow. The difference between the WSS signals is small. Consider the vesicle orientation shown in figure 7. The reduction in v_t as we proceed anti-clockwise along the membrane, from the contact region, allows a nearby recirculation to exist (to the right of the contact). This allows an inversion of the WSS in the contact region. From figure 7, this inversion occurs over a length which is small compared with the diameter of the vesicle. This observation suggests that, during the transit of an erythrocyte through a capillary or close the to lumen of a larger vessel, an inversion in the WSS signal over the length a single lumen-bound endothelial cell is effectively avoided when that erythrocyte's membrane motion is constrained to move uniformly.

We note that all our data relate to vesicles at $Re \geq 1$. The present method overcomes the key limitation in terms of physical behaviour present in our previous method [10]. However, there remains the issue of access to computations within the Stokes regime of flow, where the interfacial micro-current induced at the interface is significant.

7   Conclusion

In this article we have presented a method for applying a class of velocity-dependant forces within a multi-component lattice Boltzmann equation simulation, which is designed to recover continuum regime incompressible hydrodynamics, at $Re > 1$, where the impact of the interfacial micro-current is restricted.

This method has been applied to the problem of constraining to uniformity the tangential velocity of a vesicle membrane implemented within a recent, pure multi-component lattice Boltzmann simulation method, which avoids the use of Lagrangian boundary tracers (Phys. Rev. E. 87, 023307 (2013)). The constraint of uniform tangential velocity is carried by an ad-

15

ditional contribution to an immersed boundary force, which we derive here from physical arguments. The result of this enhanced immersed boundary force is to apply a physically appropriate boundary condition at the interface between separated lattice fluids, defined as that region over which the phase-field varies most rapidly.

The limited quantity of data collected from our enhanced vesicle boundary method are in reasonable agreement with other data obtained using related methods (e.g. T. Krüger, S, Frijters, F. Günther, B. Kaoui and J. Harting, Eur. Phys. J. 222, 177 (2013)) and underscore the importance of a correct, effective vesicle membrane condition.

It is important to emphasise that the model advanced by the work reported (Phys. Rev. E. 87, 023307 (2013)) is able to simulate many vesicles, by exploiting memory-efficient multi-component lattice Boltzmann methods already developed for immiscible drops (Phil. Trans. Roy. Soc. A. 362, 1775 (2004)). That crucial property is inherited in the present, extended model. Were that not the case, the model and its extensions reported here might be viewed as unnecessary.

Appendices

A   Figures and Captions and Tables

Table 1: Convergence of $R(j)$

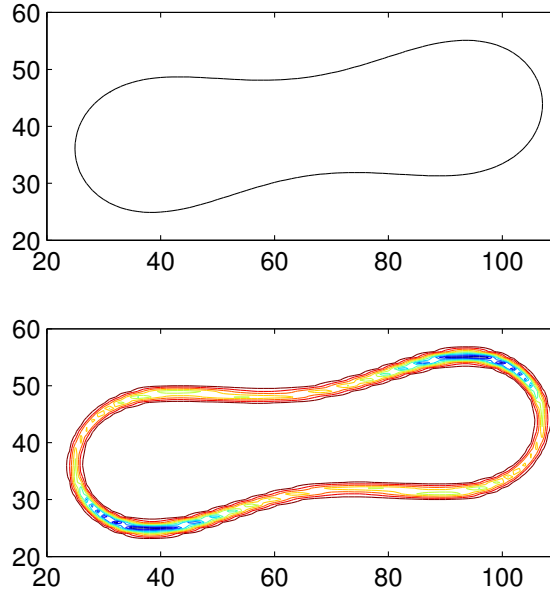| j	$R(j)$	$\log_{10}(R(j))$
1	3.97×10^{-1}	-0.401
2	1.89×10^{-1}	-0.723
3	2.35×10^{-4}	-3.630

Figure 1: The tangential component of membrane velocity for a sheared vesicle without control of the tangential membrane motion i.e with global length conservation. Upper panel shows the locations of the contour $\rho^N = 0$. Using only the normal force distribution of equation 6, the 2D vesicle with perimeter depicted in the upper panel is embedded within a sheared fluid, with its top layer moving right. The bottom panel shows equally spaced contours of clockwise-positive tangential velocity, v_t, in the region of the interface. v_t clearly varies significantly (approx 50 %) over the length of the membrane.
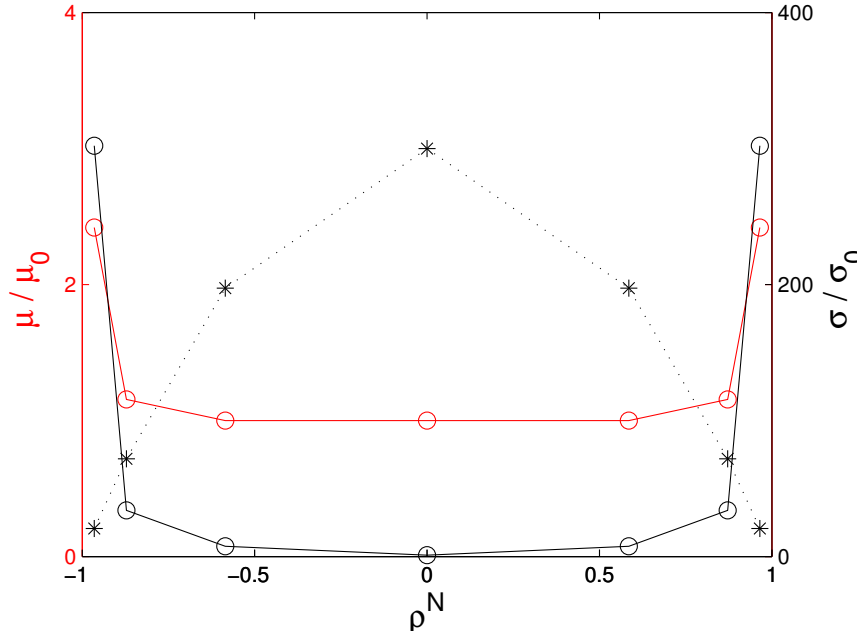
Figure 2: Variation of the tangential velocity with the constraint force $\underline{F}'$ in equation 22 applied. The tangential velocity in the interfacial region was interpolated onto phase field contours $\rho^N = 0, \pm 0.585, \pm 0.872, \pm 0.965$ The mean, μ, (red open circles, right ordinate) and standard deviation, σ (black open circles, right ordinate) on each contour is plotted against ρ^N. A representation of the weight function is also shown (black asterisks) for reference. The mean (standard deviation) data is normalised to μ_0, the mean, (σ_0, standard deviation) on contour $\rho^N = 0$. All lines are added only to guide the eye.
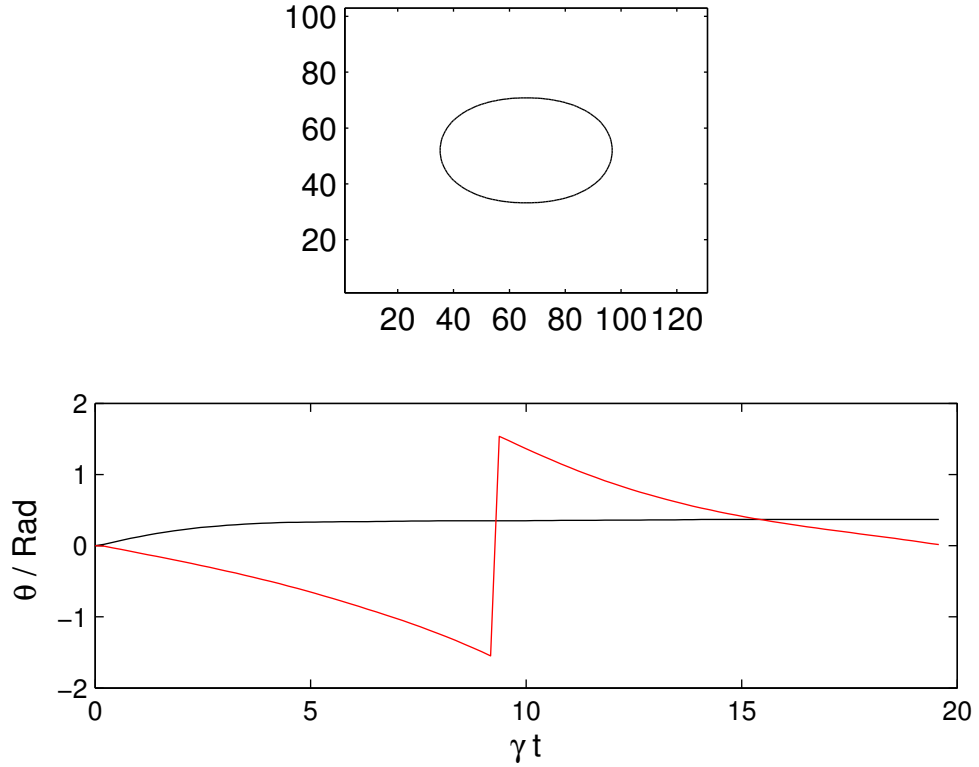
Figure 3: Top figure : the initial, mildly-deflated vesicle represented within the simulation domain. Lower figure: the angular position of the long axis of vesicle as a function of time, relative to the direction of unperturbed flow. Note that time has been non-dimensionalized using $\dot{\gamma}$. The black (red) line corresponds to $\Lambda = 1$ ($\Lambda = 12$).
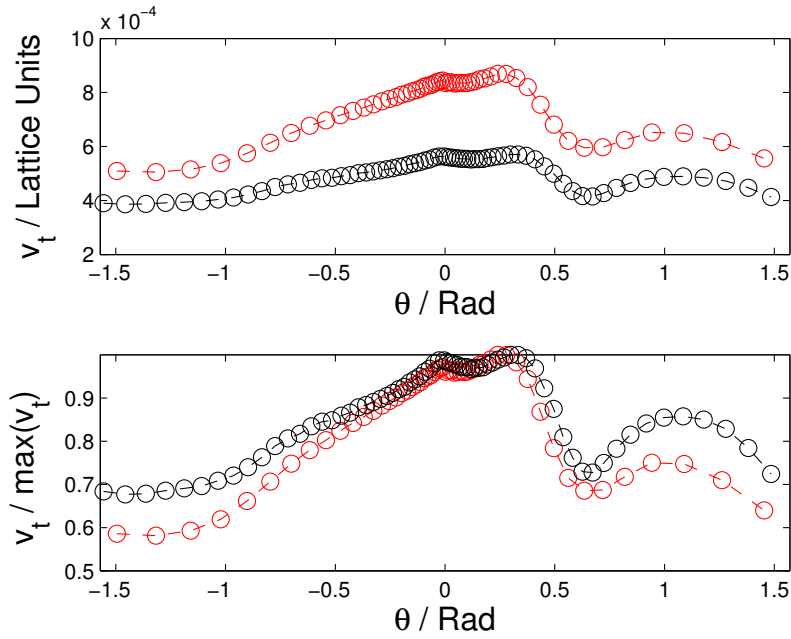
Figure 4: Plots of v_t with θ for two collapsed, tumbling vesicles $\alpha = 0.7$, (red circles) $\alpha = 0.8$ (black circles). Both vesicles have $\Lambda = 1$. Data were obtained at equal intervals of time hence the local density of points is an indication of the angular velocity of the vesicle. The tumbling motion is accompanied by shape changes, note. See also companion figure 5 below.
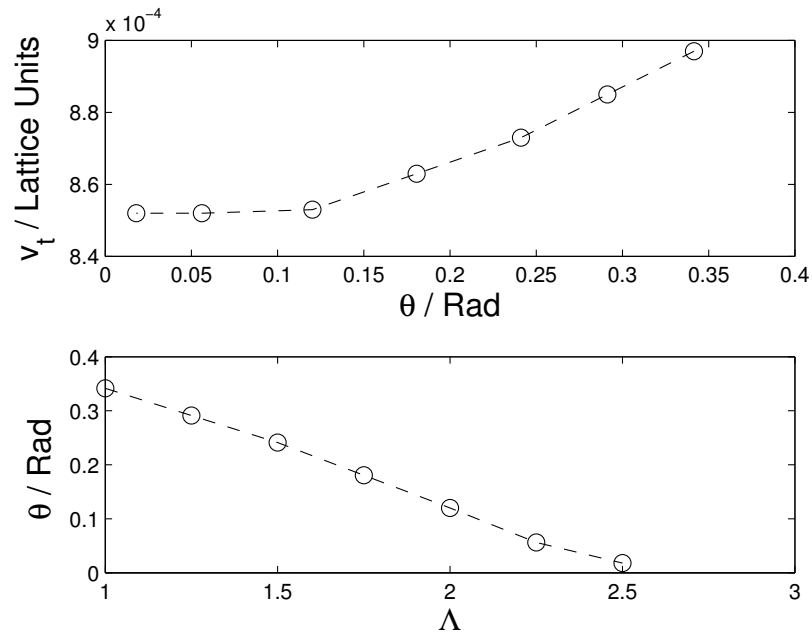
Figure 5: Plot of v_t vs. θ for sheared vesicles with $\alpha = 0.93$, at a range of $\Lambda \in [1, 2.5]$. The steady inclination reached by the vesicle systems shown here was identified in computations when $\frac{d\theta}{dt} = 0$).
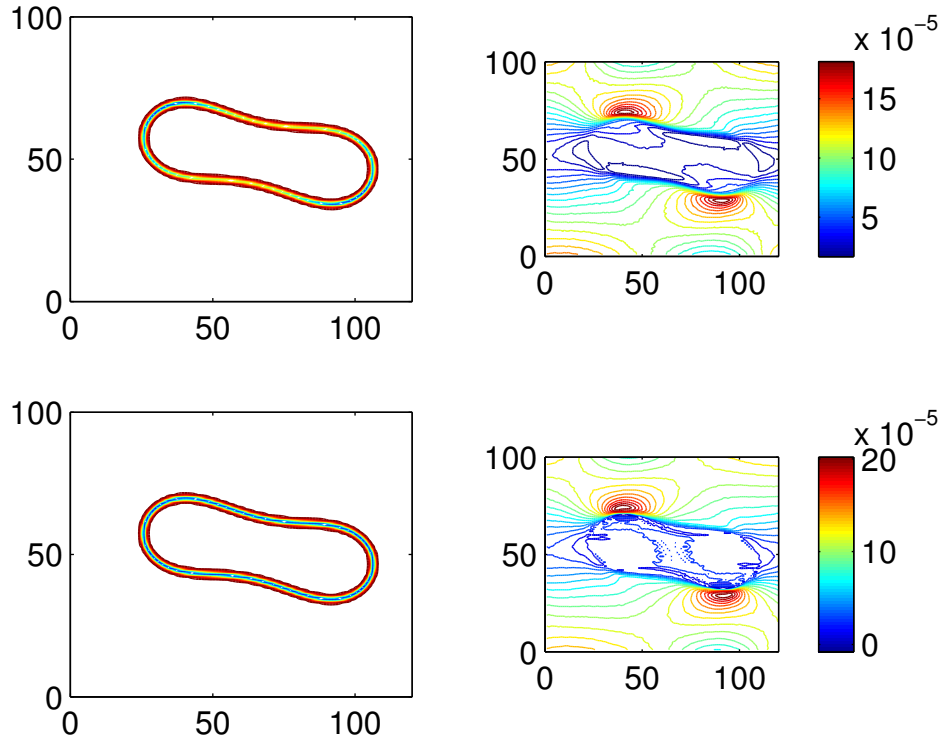
Figure 6: Data for a tumbling vesicle with that vesicle orientated approximately parallel with the direction of undisturbed horizontal shear flow. First row, top left panel: v_t without the constraint of constant tangential motion, top right panel: WSS i.e. $\frac{\partial v_x}{\partial y}$ without the constraint of constant tangential motion. Second row, top left panel: v_t with the constraint of constant tangential motion, second panel: WSS i.e. $\frac{\partial v_x}{\partial y}$ with the constraint of constant tangential motion. That is, the bottom row shows corresponding data for a membrane subject to our constraint force.
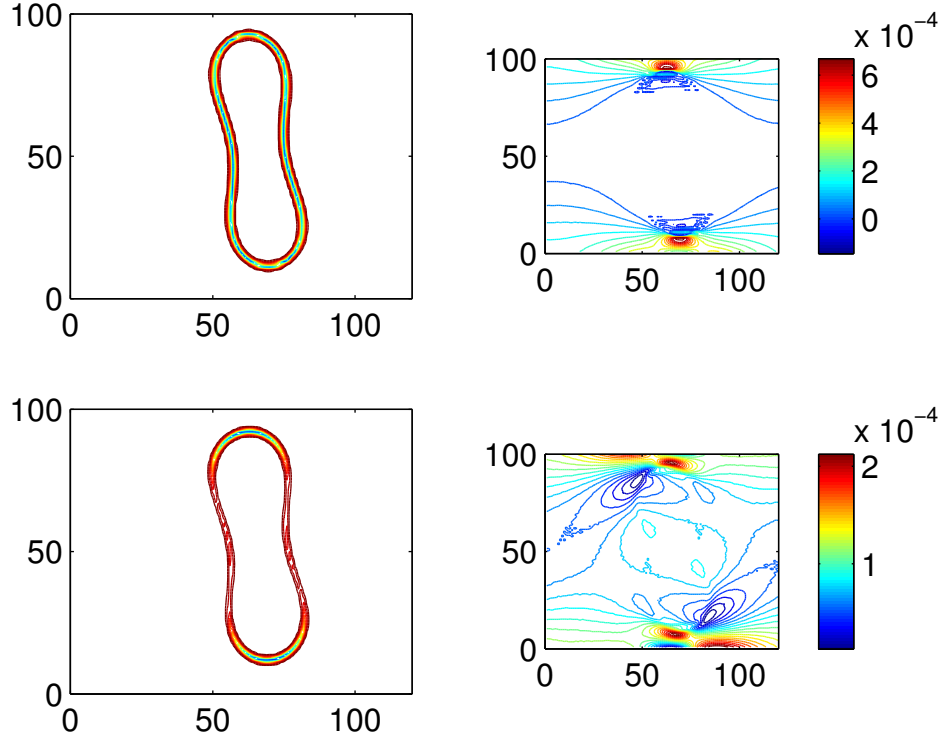
Figure 7: Data for a tumbling vesicle with that vesicle approximately perpendicular to the direction of undisturbed horizontal shear flow. First row, top left panel: v_t without the constraint of constant tangential motion, top right panel: WSS i.e. $\frac{\partial v_x}{\partial y}$ without the constraint of constant tangential motion. Second row, top left panel: v_t with the constraint of constant tangential motion, second panel: WSS i.e. $\frac{\partial v_x}{\partial y}$ with the constraint of constant tangential motion. The bottom row shows corresponding data for a membrane subject to our constraint force.

References

[1] D. McDonald, W. W. Nichols, M. F. O'Rourke and C. Vlachopoulos, *McDonalds Blood Flow in Arteries, Theoretical, Experimental and Clinical Principles*, Ed 6, CRC press (2011)

[2] C. S. Peskin, J. Comput. Phys. 25, 220 (1977).

[3] J. M. Skotheim and T. W. Secomb, Phys. Rev. Lett. 98, 078301 (2007).

[4] T. W. Secomb, R. Hsu, and A. R. Pries, Microcirculation 9, 189 (2002).

[5] B. Kaoui, G. Biros, and C. Misbah, Phys. Rev. Lett. 103, 188101 (2009).

[6] B. Kaoui, G. H. Ristow, I. Cantat, C. Misbah, and W. Zimmermann, Phys. Rev. E 77, 021903 (2008), and references therein.

[7] B. Kaoui, J. Harting, and C. Misbah, Phys. Rev. E 83, 066319 (2011).

[8] J. Zhang, P. C. Johnson, and A. S. Popel, Phys. Biol. 4, 285 (2007).

[9] T. Krüger, F. Varnik, and D. Raabe, Comp. Math. Appl. 61, 3485 (2011).

[10] I. Halliday, S. V. Lishchuk, T. J. Spencer, G. Pontrelli and C. M. Care Phys. Rev. E. 87, 023307 (2013).

[11] M. M. Dupin, I. Halliday and C. M. Care, Medical Engineering and Physics 28 13 (2006).

[12] M. M. Dupin, I. Halliday and C. M. Care, Phil. Trans. Roy. Soc. A. 362, 1775 (2004).

[13] V. Bennett and D. M. Gilligan, Ann. Rev. Cell. Biol. 9 27 (1993)

[14] R. Skalak et. al., Biophysics. J. 13 245 (1973)

[15] T. M. Fischer, Biophysics. J. 86 3304 (2004)

[16] S. V. Lishchuk, C. M. Care and I. Halliday, Phys. Rev. E 67(3), 036701(2), (2003).

[17] I. Halliday, A. P. Hollis and C. M. Care, Phys. Rev. E, 76 026708 (2007).

[18] U. D'Ortona, D. Salin, M. Cieplak, R. B. Rybka and J. R. Banavar Phys. Rev. E 51, 3718 (1995)

[19] P. M. Chaikin and T. C. Lubensky, Principles of Condensed Matter Physics, Cambridge University Press (2000) ISBN : 9780521794503

[20] D. Salac and M. J. Miksis, J. Fluid Mech 711 pp122 (2012)

[21] B. Kaoui, T. Krüger, and J. Harting, Soft Matter 8, 9246 (2012)

[22] B. Kaoui and J. Harting, Rheologica Acta 55 (6) pp465 (2015)

[23] X. He, S. Chen and G. D. Doolen, J. Comp. Phys. 146 282 (1998).

[24] Z. Guo, C. Zheng and B. Shi, Phys. Rev. E, Vol 65 046308 (2002).

[25] Y. H. Qian, D. d'Humières and P. Lallemand, Europhys. Lett. **17**, 479 (1992).

[26] Z. Guo and T. S. Zhao, Phys. Rev. E. 66, 036304 (2002)

[27] J. Beaucourt, F. Rioual, T. Séon, T. Biben and C. Misbah, Phys. Rev. E, 69, 011906 (2004)

[28] P. Nithiarasu and K. Ravindran, Comput. Methods. Appl. Mech. Eng., 165 147 (1998).

[29] S. Succi, *The lattice Boltzmann Equation for Fluid Mechanics and Beyond*, Clarendon Press (2001).

[30] T. Krüger, S, Frijters, F. Günther, B. Kaoui and J. Harting, Eur. Phys. J. 222, 177 (2013).